iScience, Volume *23*

Supplemental Information

AFM Analysis Enables Differentiation between Apoptosis, Necroptosis, and Ferroptosis in Murine Cancer Cells

Louis Van der Meeren, Joost Verduijn, Dmitri V. Krysko, and André G. Skirtach

Supplemental figures:

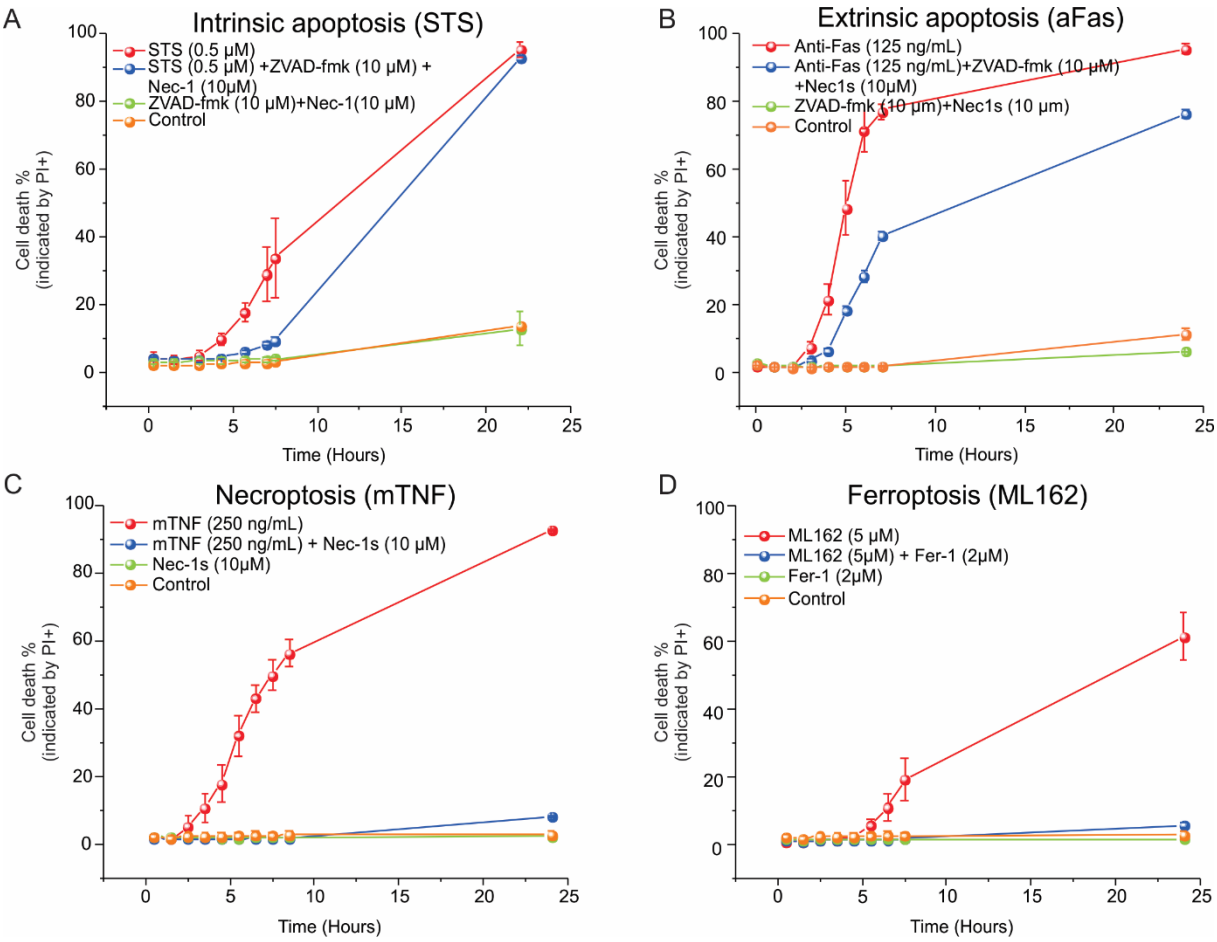

Figure S1 related to Figure 1 Cell death (RCD) time analysis of the induction/inhibition experiments to test if inducers stimulate the proclaimed cell death modality analyzed by wide-field fluorescence microscopy.

The percentage of dead cells was calculated by counting the percentage of cells marked by Propidium Iodide (PI), which is a nuclear dye that can only enter cells after membrane permeabilization has occurred. By adding the specific inhibitor targeting a protein essential in initiating the respective process of regulated cell death (RCD), the cell death process can be inhibited or delayed. In the performed experiments, all inhibitors were added 30 minutes before cell death inducers. (**A**) The addition of pan-caspase inhibitor zVAD-fmk delays extrinsic apoptotic cell death after the induction with STS by inhibiting caspase activation, however, a complete inhibition is not possible since caspase inhibition eventually leads to cell death as was proven in previous research(Wu et al., 2011). (**B**) zVAD-fmk addition leads to a delay of intrinsic apoptosis after the induction with Anti-Fas antibody, by inhibiting caspases. However, similar to the observation in extrinsic apoptosis no complete inhibition is possible due to the occurrence of zVAD-fmk induced necroptosis. (**C**) Necrostatin-1s inhibits RIPK1 activation, which essential in the execution of necroptosis. Here the addition of Nec1s successfully inhibits necroptotic cell death after induction with mTNF (Takahashi et al., 2012). (**D**) Ferrostatin-1 is a lipid-ROS scavenger that allows inhibiting ferroptotic cell death by targeting lipid ROS produced after the addition of ML162 (Dixon et al., 2012). In the performed experiments, it is observed that ferroptosis was effectively inhibited by adding Fer-1.

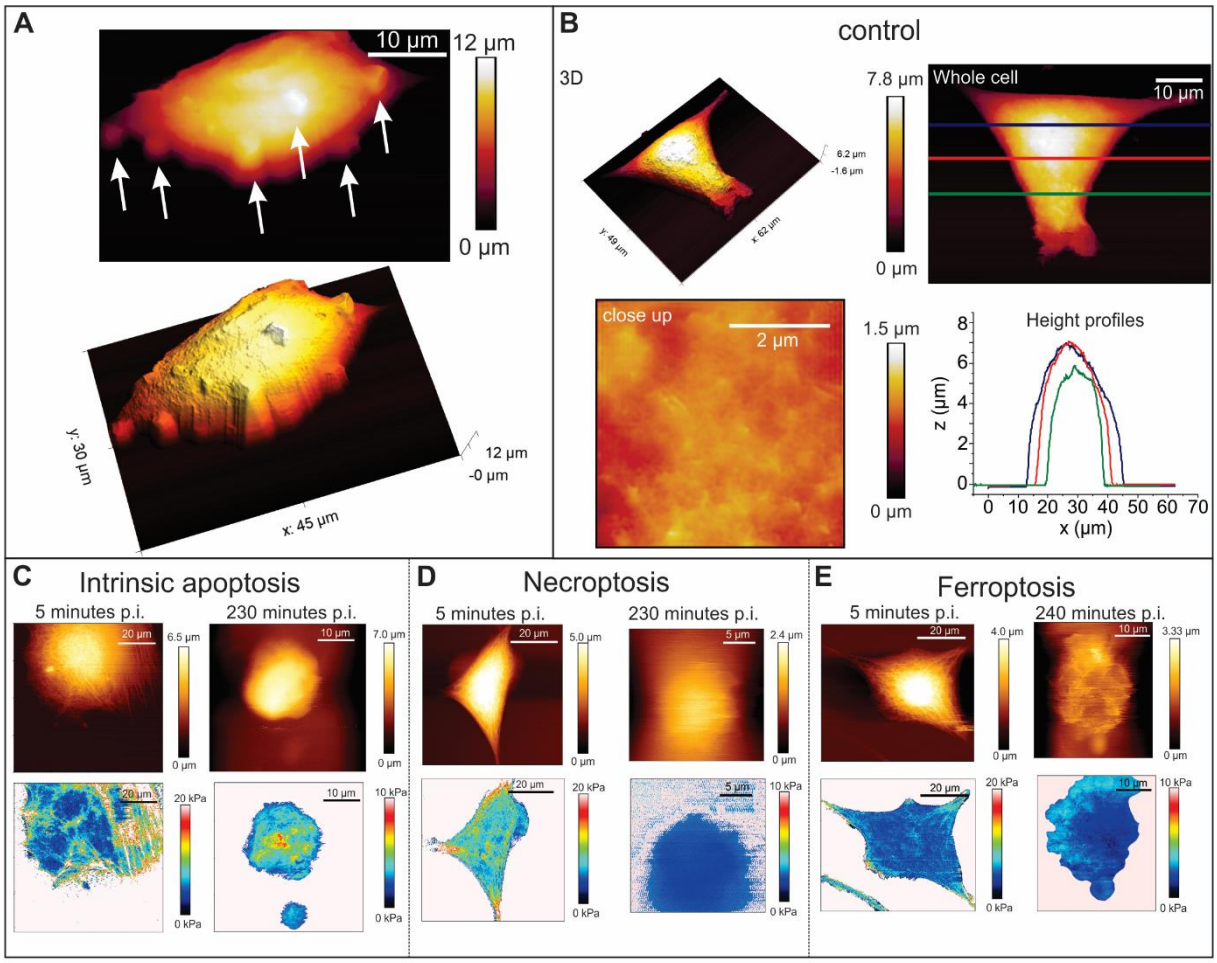

Figure S2 related to Figure 2 Morphological AFM analysis of control cells.
(**A**) Top: 3D (left) and 2D (right) of a control. Bottom left: control cells, imaged with confocal microscopy, exhibit the typical morphology of live L929sAhFas cells (blue stain: Hoechst33342 DNA stain). Bottom right: close up of the membrane of a control cell that shows a smooth membrane surface without any remarkable disruptions. (**B**) Additional height image (2D and 3D) showing the typical morphology of a ferroptotic cell. White arrows: circular protrusions originating from the cellular membrane that were frequently observed after induction of ferroptotic cell death**.** (**C-E**) Example of live imaging of cells during the process of RCD (Left to right: Intrinsic apoptosis, necroptosis, and ferroptosis). Top row: height image, Bottom row: pixel-by-pixel Young's modulus mapping.

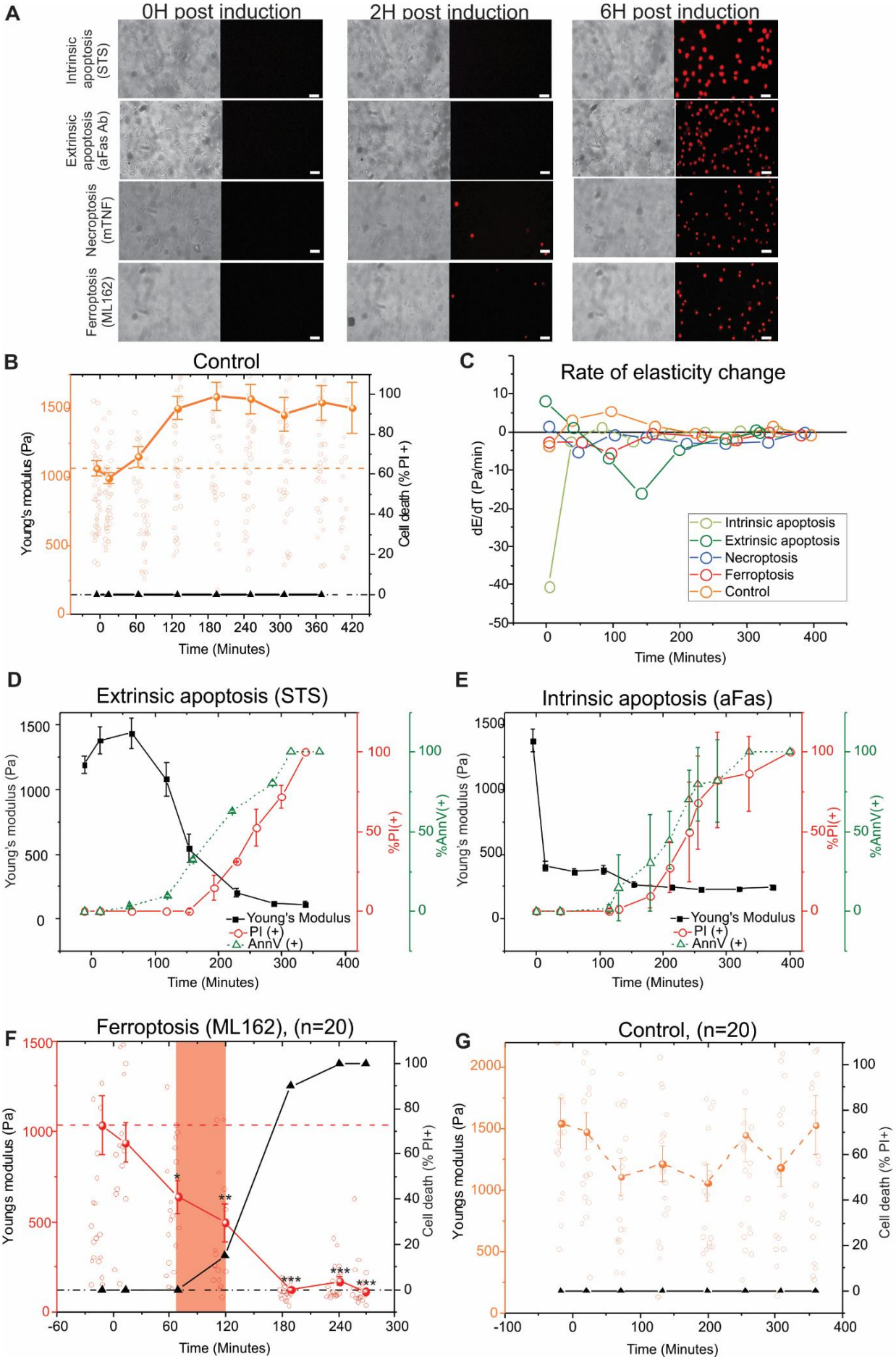
A
0H post induction
2H post induction
6H post induction
Intrinsic apoptosis (STS)
Extrinsic apoptosis (aFas Ab)
Necroptosis (mTNF)
Ferroptosis (ML162)
B
Control
Young's modulus (Pa)
Cell death (% PI +)
Time (Minutes)
C
Rate of elasticity change
dE/dT (Pa/min)
Intrinsic apoptosis
Extrinsic apoptosis
Necroptosis
Ferroptosis
Control
Time (Minutes)
D
Extrinsic apoptosis (STS)
Young's modulus (Pa)
%PI(+)
%AnnV(+)
Young's Modulus
PI (+)
AnnV (+)
Time (Minutes)
E
Intrinsic apoptosis (aFas)
Young's modulus (Pa)
%PI(+)
%AnnV(+)
Young's Modulus
PI (+)
AnnV (+)
Time (Minutes)
F
Ferroptosis (ML162), (n=20)
Youngs modulus (Pa)
Cell death (% PI+)
Time (Minutes)
G
Control, (n=20)
Youngs modulus (Pa)
Cell death (% PI+)
Time (Minutes)

Figure S3 related to Figure 3. Fluorescence microscopy analysis of RCD.

(**A**) (i.e. membrane permeabilization, PI^+) was during AFM (Scale bar = 20 μm). (**B)** Dynamics of the mechanical properties in the control cells. The left Y-axis indicates elasticity, right Y-axis cell death as measured by the percentage of PI^+ cells. Error bars indicate the standard error of means (SEM). An increase can be noticed in elasticity during the initial timepoints of the experiments that can be noticed. This is most likely caused by suboptimal conditions during the transferring samples; however, this is stabilized during the later stages of the experiments. (**C**) Comparison of the rates of elasticity changes during the process of RCD (obtained by taking the first-order derivative of the elasticity during the process of cell death for each of the investigated modality). Lower values indicate faster decrease rates. (**D-E**) Time dependence of the elasticity experiments superimposed on fluorescence measurements combining both Propidium iodide and Annexin V labels to indicate the late and early cell death, respectively in (**D**) extrinsic apoptosis and (**E**) intrinsic apoptosis. (**F**) Dynamics of cellular elasticity during ferroptosis, measured in an MCA205 cell line. A colored rectangle indicates the delay between the first significant decrease of cellular elasticity and the first signal of cell death (PI^+). Significance was calculated using the Wilcoxon rank-sum test (*p <0.05, **p<0.01, ***p<0.001, error bars indicate SEM). (**G**) dynamics of cellular elasticity in the control MCA205 cells.

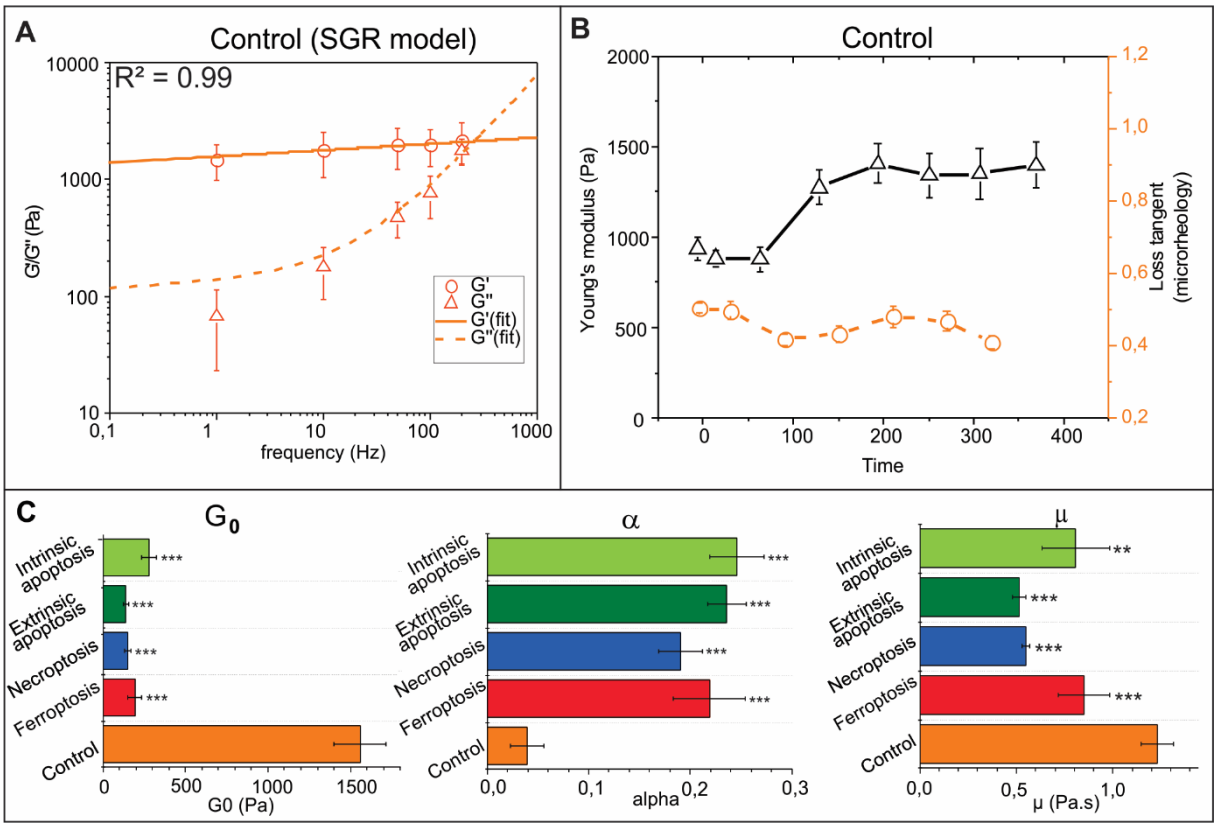

Figure S4 related to Figure 4. Microrheological analysis of RCD.

(**A**) SGR model fit over a frequency range from 1 to 200 Hz in control cells, G' indicates shear storage and G'' indicates shear loss. The points indicate points obtained by measurements while the lines refer to the values of the fitted models, R^2 value in the top left corner indicates the correlation of the measured data with the proposed SGR model, this high correlation allows to use the interpretation of this model for further analysis. Error bars show standard deviation (n=10). (**B**) A pairwise comparison of elasticity versus dynamic in cellular microrheology (represented by a loss tangent) the loss tangent remains stable throughout the experiment. The error bars in the loss tangent graphs indicate the standard error of means (SEM) n=30. (**C**) Bar graphs comparing the parameters resulting from the SGR models, G_0 scaling factor (Pa), alpha: power-law exponent, μ: Newtonian viscosity factor (Pa/s) (detailed explanation of these parameters can be found in Supplementary notes 2). Error bars indicate standard deviation (n=5), significance was calculated using a two-sample Student's t-test (**p<0.01, ***p<0.001).

Table S1 related to Figure 3. Statistical comparison of the time delay between AFM detection and the appearance of the first fluorescent signal. The onset of RCD onset detection with AFM compared to PI+ signal, (statistical significance is compared to control cells ***p<0.001, p-values were obtained using a Wilcoxon rank-sum test).

RCD	First significant elasticity decrease (minutes post induction)	p-value (vs. Control)	First increase PI^+ signal (minutes post-induction)	**Δt (min)**
Intrinsic apoptosis	14	7.85E-15 ***	180	**166**
Extrinsic apoptosis	153	7.18E-08 ***	193	**40**
Necroptosis	83	7.80E-04 ***	182	**99**
Ferroptosis	81	2.07E-05 ***	236	**155**

Table S2 related to Figure 3. Rate of elasticity change per measured time point. Numerical data used to visualize the graph shown in Figure S1C

Intrinsic apoptosis		**Extrinsic apoptosis**		**Necroptosis**		**Ferroptosis**	
Time (minutes)	dE/dt (Pa/min)	Time (minutes)	dE/dt (Pa/min)	Time (minutes)	dE/dt (Pa/min)	Time (minutes)	dE/dt (Pa/min)
4	-40.35963	1	14.52216	2.5	1.57944	3.5	-2.68251
36.75	-2.52451	38.5	-2.46024	47.5	-5.13107	52	-2.66814
82.5	1.26965	91	-6.13272	102	-0.64558	97	-5.52833
129.75	-2.24311	136	-14.76087	149	-1.44514	158	-0.41409
183.75	-0.33762	173.5	-4.94972	208.5	-3.05878	232	-1.14444
237	-0.2579	211	-4.37092	268	-3.1066	283.5	-1.94438
290.25	0.04891	258	-1.78066	331.5	-2.54441	333.25	-0.2535
346.25	0.10415	312.5	0.36987	386	-0.04629	380	-0.77324

Table S3 related to Figure 3. Statistical analysis of the rate of the elasticity change. Significance test for the rate of elasticity decrease in each of the RCD modalities, (***p<0.001, p-values were calculated using a two-sample Student's t-test).

RCD	Max rate of elasticity change (Pa/min)	Sd (±)	Vs. intrinsic apoptosis	Vs. extrinsic apoptosis	Vs. necroptosis	Vs. ferroptosis
Intrinsic apoptosis	**-42.27**	**26.97**	1	3.04e-7 ***	4.01e-13 ***	9.79e-14 ***
Extrinsic apoptosis	**-16.21**	**14.58**	3.04e-7 ***	1	3.75e-5 ***	3.79e-6 ***
Necroptosis	**-5.13**	**7.46**	4.01e-13 ***	3.75e-5 ***	1	0.27
Ferroptosis	**-3.57**	**6.07**	9.79e-14 ***	3.79e-6 ***	0.27	1

Table S4 related to figure 4 Statistical comparison of the delay between elasticity and microrheology changes during RCD modalities. Overview table comparing the delay between a significant change in elasticity versus significant change` in loss tangent for each of the regulated cell death modalities (statistical significance is compared to control cells * p <0.05, ** p<0.01, *** p<0.001).

RCD	First significant loss tangent increase (minutes post-induction)	p-value (vs. Control)	First significant elasticity decrease (minutes post-induction)	**Δt (min)**
Intrinsic apoptosis	37.5	2.85E-10 ***	14	**23.5**
Extrinsic apoptosis	163.5	6.11E-03 **	153	**9.5**
Necroptosis	259	4.67E-03 **	83	**176**
Ferroptosis	253	4.77E-04 ***	81	**172**

Transparent methods:

Cell culture and regulated cell death induction: L929sAhFAS fibrosarcoma cells were cultured in Dulbecco's Modified Eagle Medium (LONZA, 12-604F) supplemented with 10% FBS (FisherScientific, 11591821), 1% Penicillin/streptomycin (LONZA, DE17-602E) (Vanhaesebroeck et al., 1992; Vercammen et al., 1997). Different modes of cell death were induced by adding the corresponding compounds. MCA205 cells were cultured in RPMI 1640 (LONZA, BE12-702F) supplemented with 10% FBS (FisherScientific, 11591821), 1% Penicillin/streptomycin (LONZA, DE17-602E). Extrinsic apoptosis is induced by STS (VWR, 569396-100, 1 µM), intrinsic apoptosis is induced by adding aFas antibody (Merck, 05-201, 125 ng/mL), necroptosis is induced by adding mTNF-alpha (recombinant protein from VIB Protein Service Facility, 250 ng/mL) and ferroptosis is induced by adding ML162 (SanBio, 20455-5, 10 µM). Induction of ferroptosis in MCA205 cells is induced equally as in L929sAhFas cells by adding ML162.

Cell death type confirmation experiments: For the cell death induction experiment (Figure 1S), cells were seeded in a 96 well plate (VWR, 10062-900) to a density of 10000 cells per well one day prior. To visualize the state of cells two stains were added: propidium iodide (1µg/mL; Thermofisher, P1304MP), and Hoechst33342 (1µg/mL; Thermofisher, 62249). Inhibitors were added 30 minutes before the cell death inducers (zVAD-fmk, Nec1s, and Fer1 for apoptosis, necroptosis, and ferroptosis respectively). Once inducers are added (concentrations are indicated in Figure S1), imaging is initiated. Images are made with a Nikon Ti eclipse every hour. Cell death was assessed by overlapping Hoechst 33342 (live) stain and propidium iodide (death, membrane-impermeable) stain in FIJI. During imaging, the cells are incubated at 37°C with 5% CO2.

High-resolution optical images were made on a Nikon confocal scanning laser microscope (Figure 1), in these experiments three fluorescent labels were used namely: Hoechst 33342 (DNA stain live cells, blue) (Thermofisher, 62249), Alexa fluor 488 Annexin V (phosphatidylserine exposure stain, green) (Thermofisher, A13201) and propidium iodide (DNA stain dead cells, red) (Thermofisher, P1304MP). During these experiments, cells were imaged at different time points after induction.

AFM morphological analysis: For all AFM experiments cells were seeded 1 day before the experiments on glass-bottom Petri dishes (confocal dishes) to a concentration of 55.000 cells mL^{-1}. Topographical images were acquired using the nanowizard 4™ (JPK GmbH Instruments/Bruker) in the JPK QI® mode using ATEC-CONT cantilevers, these sharp tip cantilevers (radius of curvature < 10 nm) have an increased tip height (15 µm) to avoid contact of the cantilever and the cells during imaging. Before topographical imaging, the cells were fixed at 3 hours post-induction. This time point was determined based on CLSM images. First, the dishes were washed 3 times with PBS, consequently, a 4% Paraformaldehyde (PFA, Alfa Aesar™, 043368.9M) solution was added for 10 minutes finally the PFA solution was replaced with PBS, and in-between measurements, cells were stored at 4°C For each RCD modalities 3 areas of 5 by 5 µm were analyzed on 5 different cells (n=15 total). Based on this data the average roughness (Ra), root means square roughness (Rq), and the peak-to-valley roughness (Rt) was calculated for each RCD modality. Significance compared to control was analyzed using a two-sample Student's t-test, since the roughness data have a normal distribution.

AFM elasticity analysis: For all AFM experiments, cells were seeded 24 hours before the experiments on glass-bottom Petri dishes, treated for increased attachment (VWR, 75856-740), to a concentration of 55.000 cells/mL. The AFM instrument used during all experiments is the nanowizard 4™ with a manual stage (JPK GmbH Instruments/Bruker). To ensure optimal conditions during the live-cell mechanical measurements an incubator was constructed around the AFM instrument allowing control of temperature and CO_2 (37°C and 5% CO_2), all force curves were acquired in contact mode using a colloidal probe, containing a spherical tip of 5 µm diameter (CP-qp-SCONT-BSG, force constant 0.1 N m^{-1}) and using a setpoint of 2 nN at 2 µm/s. Elasticity measurements were performed 5 minutes before and 15 minutes after adding the cell death inducer. The time at which the inducer is added is set as 0 minutes (which means the first measurement occurs at approximately -5 minutes). After the initial points, every 30 minutes measurements were performed. These measurements were continued until the end stage of cell death was reached for all cells in the experiments as was indicated by PI positivity (at later timepoints cells were detached and flow away rendering localization impossible). At each time point, three consecutive force curves were collected from 50 cells divided over 3 experiments (measurements were aimed above the nucleus). Simultaneously with the AFM measurements fluorescent markers added to verify cellular status, here PI was

used to indicate a late stage of cell death. To obtain Young's modulus from the force curves a Hertz model adjusted for spherical indenters is used (equation 1, using a Poisson ratio of 0.5), in the JPK data processing software (JPK, Germany; Butt et al., 2005). Young's modulus calculations were based on 400 nm indentation assuming an average cell height of 5 µm which increases as cells start to swell up and detach. (<10% of the maximum cellular height).

$$F = \frac{E}{1-\nu}\left[\frac{a^2+R^2}{2}\ln\left(\frac{R+a}{R-a}\right) - aR\right] \quad (equation\ 1)$$

$$(R = radius\ of\ the\ sphere, a = radius\ of\ contact\ circle)$$

$$\delta = \frac{a}{2}\ln\left(\frac{R+a}{R-a}\right)$$

$$(\delta = indentation\ depth = vertical\ tip\ position)$$

Elasticity experiments on MCA205 cells were performed identically as for the L929sAhFas cells, here 20 cells were analyzed over 2 experiments.

AFM microrheology measurements: To gain information on the viscoelastic properties of cells, microrheological measurements were performed. In these measurements, the force reaction toward small amplitude oscillating forces (at low frequencies) that are applied at the membrane are analyzed. For these measurements, qp-BIO-AC chips were used and more specifically the CB3 cantilever, with a 30 nm tip (force constant = 0.06 N m^{-1}). An initial set-point of 400 pN was chosen to approach the cells, during the oscillations in the experiments were performed with an amplitude of 20 nm at frequencies ranging between 1 and 100 Hz (20 oscillation cycles). To follow the loss tangent dynamics over time, three consecutive microrheology measurements were performed on a total of 30 cells at each time point, at the frequency of 100Hz for 20 cycles (10 cells per experiment). Calculations of the storage and the loss moduli were performed in JPK data processing software, based on calculations adapted from a previous paper on microrheological measurements on live cells(Alcaraz et al., 2003). To accommodate for influences originating from the cantilever's geometry, first, the deviation from the 90° phase shift in a liquid environment and the hydrodynamic drag coefficient was calculated and incorporated into the measurements ($PZT\text{-}lag = 5.4°,\ b(h_0) = 3.3e\text{-}6$). Fitting the microrheological data to the soft glassy rheology model was performed by non-linear fitting in OriginPRO 2020.

A common way to determine the microrheological properties of soft materials is by determining the shear modulus (G*(w)). This data can be obtained by performing oscillation experiments on the surface of the material and determining the complex ratio between the applied stress and the resulting strain. The shear modulus can be split into a real and an imaginary part which represents respectively the stored energy (G') and the energy dissipated inside the material (G''), these values can be calculated using Equation 2. The ratio between these two parts (G''/G', also referred to as the loss tangent) relates to how a material leans more towards a liquid- or solid-like mechanical behavior (Alcaraz et al., 2003). From a multitude of different microrheological researches, it seemed that the soft glassy rheological model is a very useful model to understand the cytoskeletal rheology, this model, the equation for this model is shown in equation S2(Kollmannsberger and Fabry, 2009). To take into account, the phase shift due to drag between the cantilever and the liquid, the piezo-lag, and the hydrodynamic drag ($b(h_0)$) are calculated (Supplemental Figure N2).

$$G^*(\omega) = G'(\omega) + iG''(\omega) = \frac{1-\nu}{3\delta_0 \tan(\theta)} \left(\frac{F(\omega)}{\delta(\omega)} - i\omega b(h_0) \right) \text{ (Equation 2)}$$

$$G^* = G_0 \left(1 + i \, tan\left(\theta \, . \frac{\pi}{2} \right) \right) (\omega)^{\alpha} + i\mu\omega \text{ (Equation 3)}$$

G_0: scaling factor (Pa), α: power-law exponent, μ: Newtonian viscosity value (Pa.s), ϑ: phase shift, $b(h_0)$: hydrodynamic drag coefficient, ω: oscillation frequency, $F(\omega)$: measured deflection, $\delta(\omega)$: measured height.

Fabry *et al.* suggested (Fabry et al., 2001) a physical interpretation of the power-law behavior of cells in microrheological measurements in a specific case of soft glassy materials. This interpretation represents the cytoskeleton as a glassy material, made up of structural elements in a matrix i.e. the cytoskeleton that can both interact and bind with each other (solid-like behavior) but also can reorganize and flow independently (fluid-like behavior). The soft glassy rheology model (SGR) provides three parameters namely: G0, α, and μ (Figures 2B, Figure S2A, Figure S2C; Alcaraz et al., 2003). The significantly decreased value for G0, a measure of the elasticity at the glass transition, for all RCD modalities logically supports the conclusions of the elasticity analysis. The parameter α is a measure for matrix agitation or how much the cytoskeleton differs from glass transition, i.e. solid state. This value can range from

0 (solid) to 1 (liquid). The increased value for α depicts a decrease in the interaction between the matrix components. This observation, together with the decreased value for μ, is a measure for the Newtonian viscosity indicating that at the late stages of RCD the cytoskeleton has lost most of its interactions between matrix components (solid behavior) and is more freely flowing (fluid behavior).

Cytoskeleton immunofluorescence imaging: Cells were seeded onto poly-L-lysine (Merck, A-005-C) coated coverslips (18mm, VWR, 48380-046) in a concentration of 60 000 cells mL^{-1}. One day after seeding, inducers were added in concentrations as mentioned above. At chosen time points cells were washed 3 times with PBS and consequently fixed using 4% PFA (Alfa Aesar™, 043368.9M) for 10 minutes. Cells are then permeabilized using Triton X-100. A blocking step using 2% BSA was done overnight at 4°C. Next, the cells were incubated for 3 hours with the primary antibody in a concentration of 2 μg mL^{-1} (alpha Tubulin Monoclonal Antibody (DM1A), Thermofisher, 62204). As a next step cells were incubated in a staining medium for 45 minutes which contained: Hoechst33342 (1 μg mL^{-1}), ActinRed™ 555 ReadyProbes (Thermofisher, R37112) and Goat anti-Mouse IgG (H+L) Highly Cross-Adsorbed Secondary Antibody, Alexa Fluor 488 (1 μg mL^{-1}) (Thermofisher, A-11029). Finally, after washing, the coverslips were mounted using SlowFade™ Glass Soft-set Antifade Mountant (Thermofisher, S36917).

Statistical analysis: All statistical analysis is performed in the software package RStudio. To analyze the difference in morphological roughness between different cell death modalities and control cells, a Kruskal-Wallis test was performed followed by a pairwise Wilcoxon test with Benjamini-Hochberg adjusted p-values. To compare the elasticity at different time points during the RCD process against the values for control cells, a Wilcoxon-rank sum test is used. The difference in the rate of elasticity change between RCD modalities was analyzed with a Kruskal-Wallis test followed by a pairwise Wilcoxon test with Benjamini-Hochberg adjusted p-values. The values of the loss tangent during the process of RCD were compared to those of control cells using a Wilcoxon-rank sum test at each time point.

Supplemental references:

Alcaraz, J., Buscemi, L., Grabulosa, M., Trepat, X., Fabry, B., Farré, R., and Navajas, D. (2003). Microrheology of human lung epithelial cells measured by atomic force microscopy. Biophys. J. *84*, 2071–2079.

Butt, H.J., Cappella, B., and Kappl, M. (2005). Force measurements with the atomic force microscope: Technique, interpretation and applications. Surf. Sci. Rep. *59*, 1–152.

Dixon, S.J., Lemberg, K.M., Lamprecht, M.R., Skouta, R., Zaitsev, E.M., Gleason, C.E., Patel, D.N., Bauer, A.J., Cantley, A.M., Yang, W.S., et al. (2012). Ferroptosis: An iron-dependent form of nonapoptotic cell death. Cell *149*, 1060–1072.

Fabry, B., Maksym, G.N., Butler, J.P., Glogauer, M., Navajas, D., and Fredberg, J.J. (2001). Scaling the microrheology of living cells. Phys. Rev. Lett. *87*.

Kollmannsberger, P., and Fabry, B. (2009). Active soft glassy rheology of adherent cells. Soft Matter *5*, 1771.

Takahashi, N., Duprez, L., Grootjans, S., Cauwels, A., Nerinckx, W., Duhadaway, J.B., Goossens, V., Roelandt, R., Van Hauwermeiren, F., Libert, C., et al. (2012). Necrostatin-1 analogues: Critical issues on the specificity, activity and in vivo use in experimental disease models. Cell Death Dis. *3*, e437-10.

Vanhaesebroeck, B., Decoster, E., Van Ostade, X., Van Bladel, S., Lenaerts, A., Van Roy, F., and Fiers, W. (1992). Expression of an exogenous tumor necrosis factor (TNF) gene in TNF-sensitive cell lines confers resistance to TNF-mediated cell lysis. J. Immunol. *148*.

Vercammen, D., Vandenabeele, P., Beyaert, R., Declercq, W., and Fiers, W. (1997). Tumour necrosis factor-induced necrosis versus anti-Fas-induced apoptosis in L929 cells. Cytokine *9*, 801–808.

Wu, Y.T., Tan, H.L., Huang, Q., Sun, X.J., Zhu, X., and Shen, H.M. (2011). ZVAD-induced necroptosis in L929 cells depends on autocrine production of TNFα mediated by the PKC-MAPKs-AP-1 pathway. Cell Death Differ. *18*, 26–37.